International Journal of Minerals, Metallurgy and Materials
Volume 26, Number 12, December 2019, Page 1559
https://doi.org/10.1007/s12613-019-1840-7

Effects of Sc and Zr microalloying on the microstructure and mechanical properties of high Cu content 7xxx Al alloy

Chong-yu Liu[1)], *Guang-biao Teng*[1,2)], *Zong-yi Ma*[3)], *Li-li Wei*[1)], *Bing Zhang*[4)], *and Yong Chen*[1)]

1) College of Material Science and Engineering, Guilin University of Technology, Guilin 541004, China
2) Guangdong JMA Aluminum Profile Factory (Group) Co., Ltd., Foshan 528200, China
3) Institute of Metal Research, Chinese Academy of Sciences, Shenyang 110016, China
4) State Key Laboratory of Metastable Materials Science and Technology, Yanshan University, Qinhuangdao 066004, China
(Received: 1 January 2019; revised: 5 March 2019; accepted: 6 March 2019)

Abstract: The effects of Sc and Zr microalloying on the microstructure and mechanical properties of a 7xxx Al alloy with high Cu content (7055) during casting, deformation, and heat treatment were investigated. The addition of Sc and Zr not only refined the grains but also transformed the θ-phase into the W-phase in the 7055 alloy. Minor Sc and Zr additions enhanced the hardness and yield strength of the 7055-T6 alloy by strengthening the grain boundaries and $Al_3(Sc,Zr)$ precipitates. However, a further increase in the Sc and Zr fractions did not refine the grains but instead resulted in the formation of the large-sized W-phase and primary coarse $Al_3(Sc,Zr)$ phase and subsequently deteriorated the mechanical properties of the alloys. The 7055 alloy with 0.25Sc addition exhibited the best mechanical property among the prepared alloys.

Keywords: aluminum alloys; microstructural evolution; mechanical property; grain refinement

1. Introduction

The addition of Sc and Zr into Al alloys results in the formation of a complex $Al_3(Sc,Zr)$ phase [1−3]. The primary $Al_3(Sc,Zr)$ phase several microns in size can promote heterogeneous nucleation in Al melts during solidification and subsequently refine the grains of Al castings [4]. The nano-sized $Al_3(Sc,Zr)$ phase that precipitates during a high-temperature homogenization treatment can further refine the grains of Al alloys during subsequent heat treatments and deformation because of its pinning effect on grain boundaries (GBs) [5−13]. Thus, Al alloys with Sc and Zr added have attracted considerable attention because of their fine-grained microstructures and high strength.

The 7xxx series (Al–Zn–Mg(–Cu)) alloys are widely used in the aircraft manufacturing industry because of their excellent mechanical properties, low densities, good formability, and high fracture toughness [14–17]. Adding Sc and Zr effectively improves the mechanical properties of 7xxx alloys with low Cu contents (mass ratio of Cu in the alloy less than 0.8%) through grain refinement [4,6–9]. The 2xxx series (Al–Cu base) alloys also exhibit high strength [18–20], and grain refinement induced by the addition of Sc has also been observed in these alloys [21−26]. Chen *et al*. [27] and Jiang *et al*. [28] found that the segregation of Sc atoms at the Al/θ′-phase interface inhibits the formation of large θ-phases (Al_2Cu) in Al–2.5wt% Cu alloys during aging. Thus, the mechanical properties of the 2xxx series alloys can also be improved by the addition of Sc. However, when the Cu content in the Al–Cu base alloy with Sc exceeds 5wt%, Sc dissolves into the θ-phase and induces a phase to transformation to the W-phase (AlCuSc) during the homogenization process [24–25]; the W-phase adversely affects the strength and plasticity of Al alloys. Furthermore, the formation of the W-phase consumes Sc atoms, thereby decreasing the amounts of Al_3Sc or $Al_3(Sc,Zr)$ phases present in the alloys. Thus, the strengthening effect of Sc addition in Al–Cu systems is not as remarkable as that observed in the 7xxx alloys.

Recently, 7xxx alloys with high Cu contents (higher

Corresponding authors: Chong-yu Liu E-mail: lcy261@glut.edu.cn; Zong-yi Ma E-mail: zyma@imr.ac.cn

than 2wt%) have been developed. These alloys exhibit higher strength and greater ductility than traditional 7xxx Al alloys [29–32]. However, the interaction between Sc and Cu in 7xxx Al alloys with high Cu contents has not been systematically investigated, and the effects of Sc and Zr microalloying on the mechanical properties of these alloys have not been determined.

In the present study, the effects of various Sc and Zr contents on the microstructure of an Al–Zn–Mg–Cu alloy (7055) with Cu content as high as 2.2wt% under casting, homogenization, rolling, and T6 treatment conditions are investigated. The mechanical properties of the 7055 alloy and 7055 alloy with different Zr and Sc additions (7055–*x*Zr–*y*Sc) in the T6 state are subsequently examined. The results of this study provide a basis for the compositional design of high-performance Al alloys.

2. Experimental

Ingots (7055 and 7055–*x*Zr–*y*Sc) were fabricated by casting. Their chemical compositions are shown in Table 1. The ingots were homogenized at 470°C for 26 h and rapidly quenched to room temperature by immersion in water. The ingots were then subjected to seven passes of rolling from 10 mm to 3 mm at 470°C. The samples were reheated at the prescribed rolling temperature for 3 min between passes. The rolled plates were subsequently subjected to solid-solution treatment at 470°C for 2 h and then aged at 120°C for 1 h to 60 h.

Table 1. Composition of 7055–*x*Zr–*y*Sc ingots wt%

7055–*x*Zr–*y*Sc	Zn	Mg	Cu	Zr	Sc
7055	7.82	1.95	2.24	0.16	–
7055–0.2Sc	7.80	1.94	2.24	0.16	0.2
7055–0.25Sc	7.81	1.93	2.24	0.16	0.25
7055–0.14Zr–0.15Sc	7.82	1.93	2.24	0.30	0.15
7055–0.14Zr–0.2Sc	7.82	1.95	2.24	0.30	0.20
7055–0.24Zr–0.15Sc	7.81	1.95	2.23	0.40	0.15

The microstructure of the alloys were examined by optical microscopy (OM, Leica-DMi8), scanning electron microscopy (SEM, S4800), transmission electron microscopy (TEM, JEOL-2010), and scanning transmission electron microscopy (STEM, F200X). The specimens for OM, SEM, TEM, and STEM were prepared in the rolling direction–normal direction plane of the samples. The TEM and STEM specimens were prepared by grinding to 50 μm, followed by thinning with a twinjet electropolishing apparatus in a solution of 90vol% methanol and 10vol% acetic acid at −10°C.

Vickers microhardness was measured with an EVERONE VH-5 hardness tester. The tensile properties of the samples were evaluated using an Instron 3369 testing machine. The tensile specimens were machined along the rolling direction; the tensile strain rate was 4×10^{-4} s^{-1}. The tensile specimens are illustrated in Fig. 1. Each alloy was tested three times.

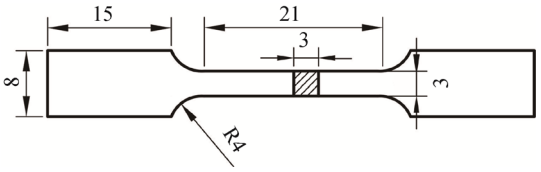

Fig. 1. Schematic of a tensile specimen (Unit: mm).

3. Results and discussion

Fig. 2 shows the OM images of the as-cast 7055 and 7055–*x*Zr–*y*Sc ingots. The grain morphologies of these ingots are listed in Table 2. A dendritic structure was observed in the 7055 ingot (Fig. 2(a)). As shown in Figs. 2(b) and 2(c), the addition of 0.2wt% or 0.25wt% Sc promoted the formation of equiaxed grains during casting, and both dendritic and equiaxed grains were observed in the 7055–0.2Sc and 7055–0.25Sc ingots. Only equiaxed grains were observed in the 7055–*x*Zr–*y*Sc ingots when the total mass fraction of Sc and Zr exceeded 0.45 (Figs. 2(d)–2(f) and Table 2).

The primary Al_3(Sc,Zr) phase promotes heterogeneous nucleation of the Al grains, thereby promoting grain refinement [6]. The density of heterogeneous nucleation sites increased with increasing the total mass fraction of Sc and Zr. Thus, refined and equiaxed grains were observed in the 7055–*x*Zr–*y*Sc ingots with high Sc and Zr additions.

Fig. 3 shows OM images of the 7055 and 7055–*x*Zr–*y*Sc ingots after homogenization. The dendritic grains in the 7055, 7055–0.2Sc, and 7055–0.25Sc ingots changed into equiaxed grains after homogenization (Figs. 3(a)–3(c)). The grain structure and size of the 7055–*x*Zr–*y*Sc ingots with high total mass fraction of Sc and Zr did not substantially change after homogenization (Figs. 3(d)–3(f)).

Fig. 4 shows the effect of Sc and Zr addition on the grain size of the homogenization-treated 7055 and 7055–*x*Zr–*y*Sc ingots. The grains of the 7055–*x*Zr–*y*Sc ingots were much finer than those of the 7055 ingot, and the average grain size of the homogenized 7055–*x*Zr–*y*Sc ingots decreased with increasing total mass fraction of Sc and Zr. No further decrease was observed when the total mass fraction of Sc and Zr exceeded 0.5.

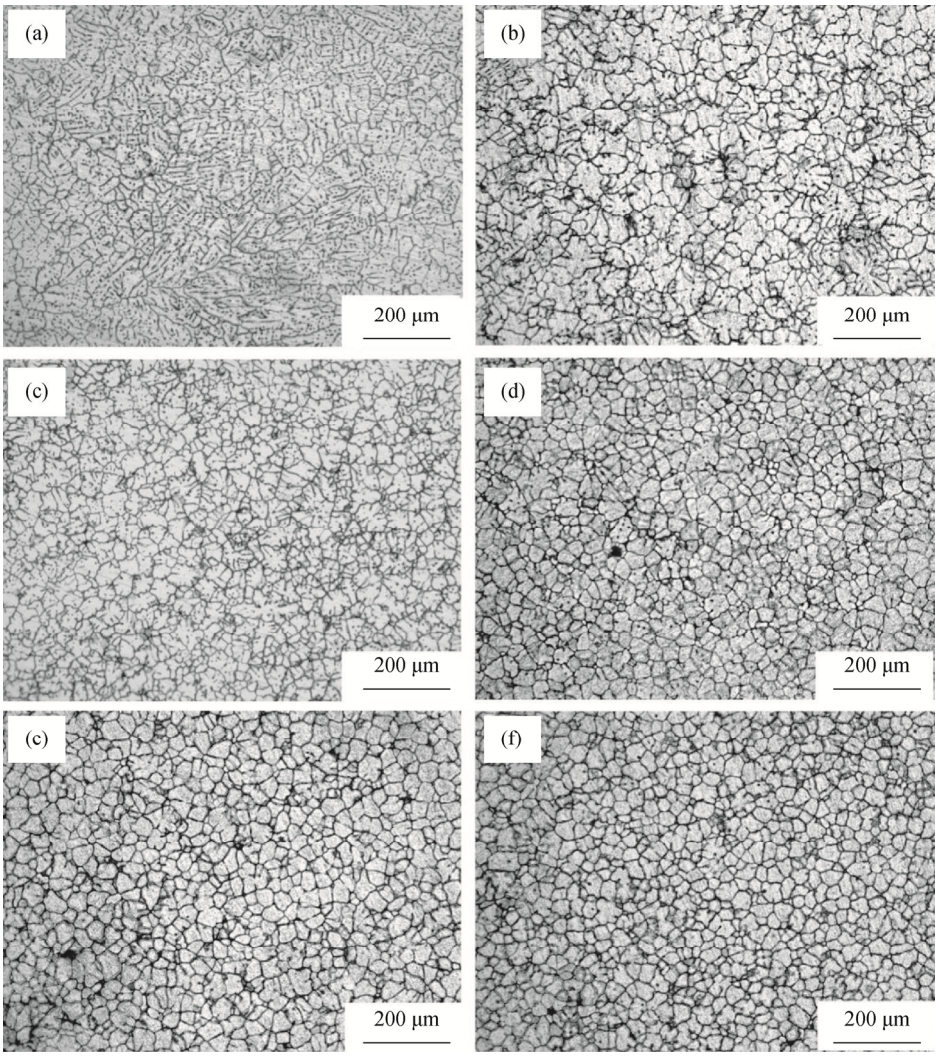

Fig. 2. OM images of as-cast ingots: (a) 7055; (b) 7055–0.2Sc; (c) 7055–0.25Sc; (d) 7055–0.14Zr–0.15Sc; (e) 7055–0.14Zr–0.2Sc; (f) 7055–0.24Zr–0.15Sc.

Table 2. Grain morphologies of as-cast 7055–*x*Zr–*y*Sc ingots

7055–*x*Zr–*y*Sc	Total mass fraction of Sc and Zr / wt%	Grain morphology
7055	0.16	Dendritic
7055–0.2Sc	0.36	Dendritic, Equiaxed
7055–0.25Sc	0.41	Dendritic, Equiaxed
7055–0.14Zr–0.15Sc	0.45	Equiaxed
7055–0.14Zr–0.2Sc	0.50	Equiaxed
7055–0.24Zr–0.15Sc	0.55	Equiaxed

TEM bright-field (BF) images of the 7055 and 7055–0.25Sc ingots after homogenization are shown in Fig. 5. Nanosized particles, which were confirmed to be the Al_3Zr phase in the 7055 after heat treatment [29–32], were observed in the TEM BF images (Fig. 5(a)). The nanosized particles of the homogenized 7055–0.25Sc ingot were denser than those of the 7055 ingot after the same process (Fig. 5(b)). The chemical composition and selected-area electron diffraction (SAED) patterns indicated that the particles in the homogenization-treated 7055–0.25Sc ingot were the $Al_3(Sc,Zr)$ phase and had the same size and structure as the Al_3Zr particles in the 7055 alloy.

The homogenization treatment led to the precipitation of the nanosized $Al_3(Sc,Zr)$ phase in the Al ingot. The particles with a GB-pinning effect effectively prevented extensive grain growth in the Sc-containing Al ingots during long heat treatment at high temperature. The density of the nanosized $Al_3(Sc,Zr)$ particles increased with increasing total mass fraction of Sc and Zr. Consequently, the grain size of the homogenized 7055–*x*Zr–*y*Sc ingots decreased with increasing total mass fraction of Sc and Zr. No further grain size decrease was observed when the total mass fraction of Sc and Zr was 0.5wt% or greater.

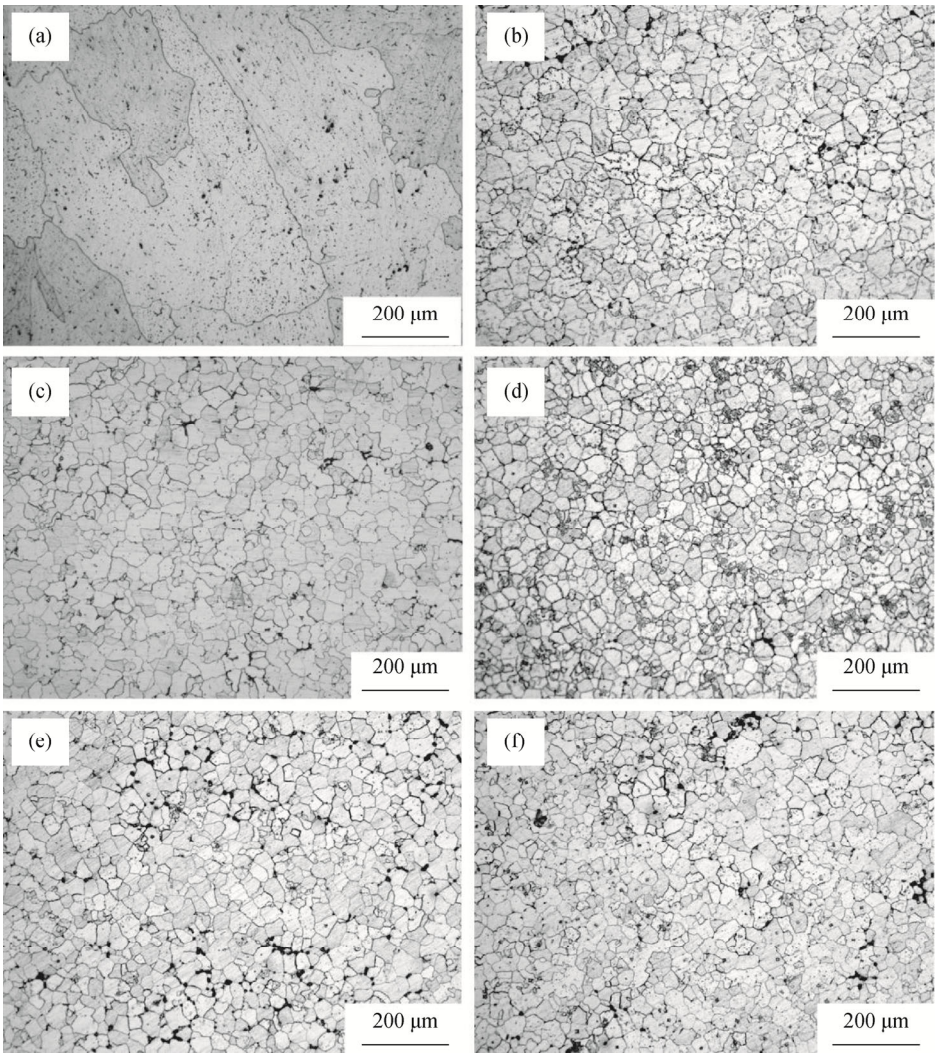

Fig. 3. OM images of homogenized ingots: (a) 7055; (b) 7055–0.2Sc; (c) 7055–0.25Sc; (d) 7055–0.14Zr–0.15Sc; (e) 7055–0.14Zr–0.2Sc; (f) 7055–0.24Zr–0.15Sc.

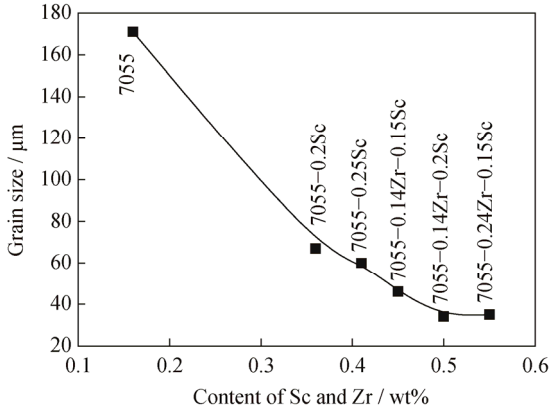

Fig. 4. Effect of total mass fraction of Sc and Zr on the average grain size of homogenized 7055–*x*Zr–*y*Sc ingots.

The SEM micrographs of the 7055 and 7055–0.25Sc ingots after homogenization are shown in Fig. 6. Micron-sized second phases were present in the two samples. The energy-dispersive X-ray spectroscopy (EDS) spectrum of particle A in Fig. 6(a) revealed that the particle was in the θ-phase. Particle B in Fig. 6(b) contained 61at% Al, 33at% Cu, 1at% Mg, and 5at% Sc, which corresponds to the W-phase.

In the Al–Cu–Sc systems with high Cu contents, Sc atoms diffused into the θ-phase and the process led to the transformation of the θ-phase into the W-phase during homogenization [24–25]. However, the W-phase was not observed in the Al–Cu–Sc alloys when the Cu content was less than 2.5wt% [21–23,27–28]. The Cu content in the 7055 was only 2.24wt%, however, this alloy also contained a high proportion of Zn and Mg atoms, which enhanced the Cu/Al ratio in this system. The extra alloying atoms drove the 7xxx to a nonequilibrium state, which promoted the phase transformation. Thus, the W-phase was formed in the Sc-containing 7055 ingots during homogenization.

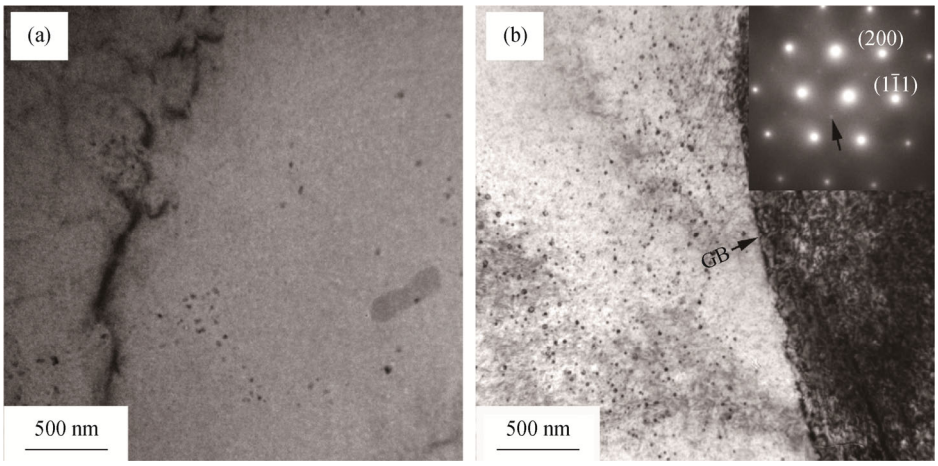

Fig. 5. TEM BF images of homogenized (a) 7055 and (b) 7055–0.25Sc ingots. The arrow in the insert of (b) denotes the diffraction spot of the $Al_3(Sc,Zr)$ phase.

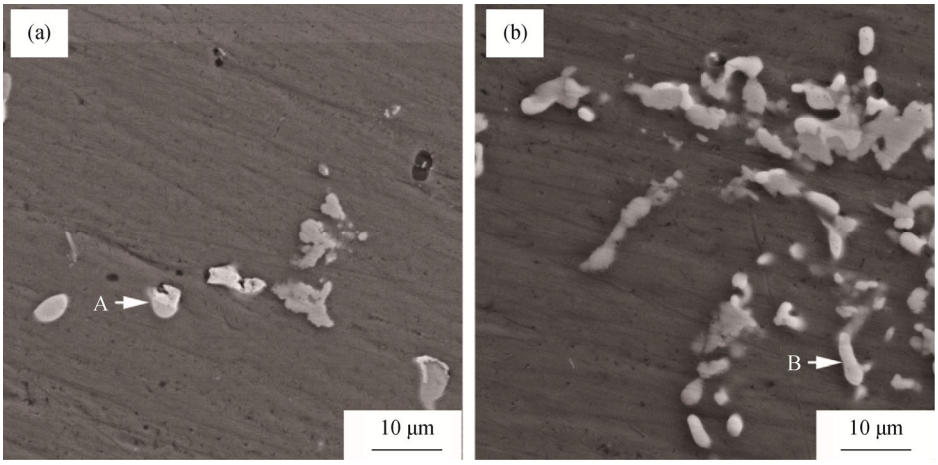

Fig. 6. SEM images of homogenized ingots: (a) 7055; (b) 7055–0.25Sc.

Jia *et al*. [24] reported that all Sc atoms could be dissolved into the W-phase in Al–4.1Cu–0.063Sc alloys. However, Gazizov *et al*. [25] found that the W-phase consumed 50% of the overall Sc atoms in an Al–5.6Cu–0.17Sc–0.12Zr alloy after homogenization. In this study, highly dense precipitated $Al_3(Sc,Zr)$ particles were observed in the homogenized 7055–0.25Sc ingot, indicating that only a small number of Sc atoms were consumed by the W-phase in the 7055–0.25Sc ingot during homogenization.

Fig. 7 shows that the Vickers hardness of the rolled plates varied with the aging time after the plates were treated with a solid-solution. The peak aging time of the 7055–*x*Zr–*y*Sc rolled plates ranged from 24 h to 26 h at 120°C, and the hardness of the 7055–*x*Zr–*y*Sc plates was higher than that of the 7055 plate at all aging time.

Fig. 8 shows OM images of the 7055 and 7055–*x*Zr–*y*Sc after the rolling and T6 treatment. Partial recrystallization occurred in the 7055 specimen, as shown in Fig. 8(a), and the fibrous grain structure generated by rolling deformation were well preserved in the 7055–*x*Zr–*y*Sc plates after the T6 treatment (Figs. 8(b)–8(f)).

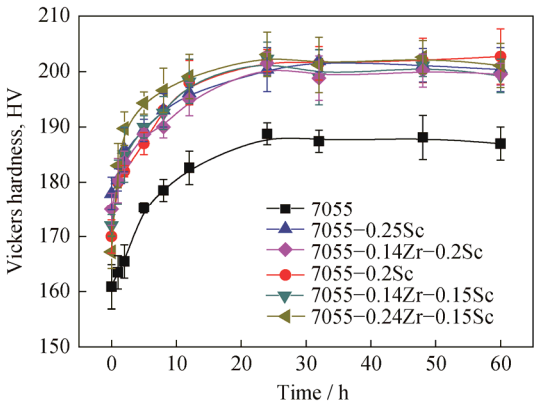

Fig. 7. Variation of Vickers hardness with aging time at 120°C for 7055–*x*Zr–*y*Sc alloys after rolling and solid–solution treatment.

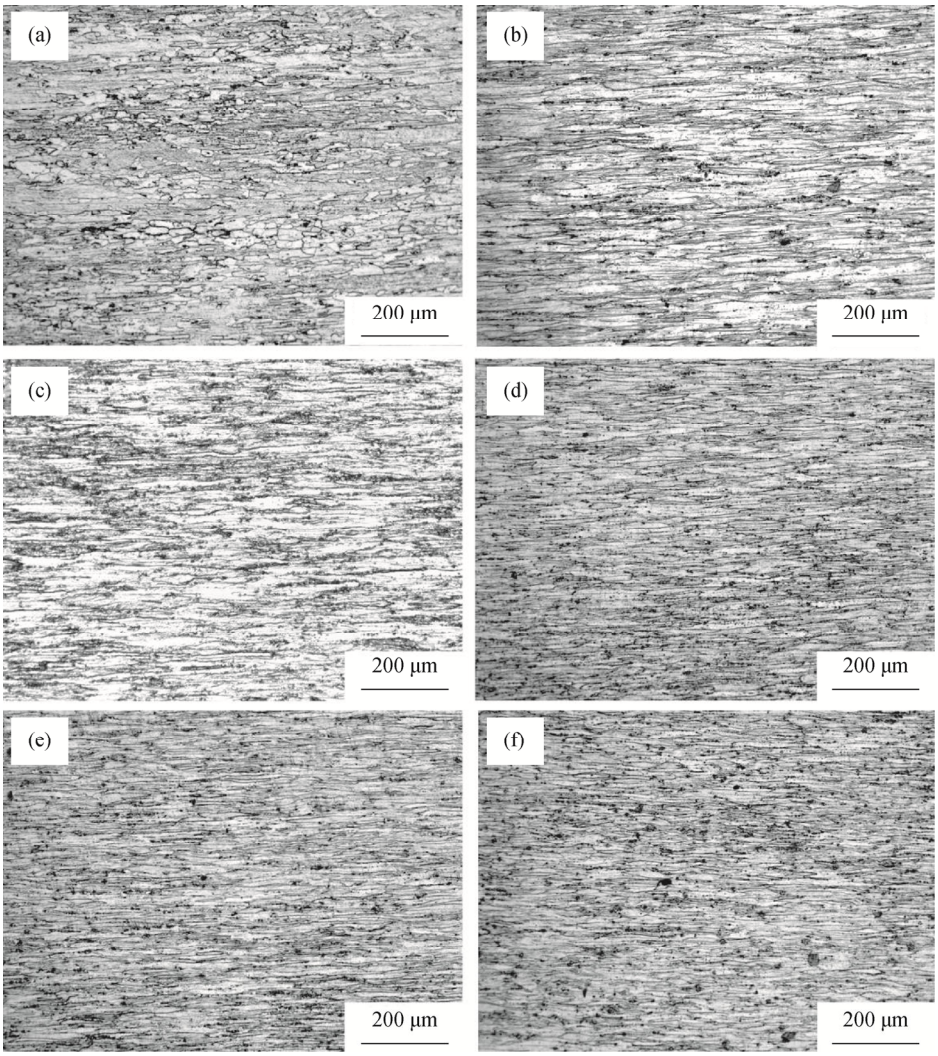

Fig. 8. OM images of the alloys after rolling and T6 treatment: (a) 7055; (b) 7055–0.2Sc; (c) 7055–0.25Sc; (d) 7055–0.14Zr–0.15Sc; (e) 7055–0.14Zr–0.2Sc; (f) 7055–0.24Zr–0.15Sc.

Fig. 9 shows the effect of the total mass fraction of Sc and Zr on the short dimension size of the elongated grains of the 7055–*x*Zr–*y*Sc rolled plates after the T6 treatment. The grain size of the samples decreased initially as the total mass fraction of Sc and Zr increased. However, when the total mass fraction of Sc and Zr was greater than 0.45wt%, the grain size did not decrease further and maintained a constant value of approximately 8 μm.

Fig. 10 shows the TEM images of the 7055 and 7055–*x*Zr–*y*Sc rolled plates after the T6 treatment. Highly dense η′ precipitates and Al_3Zr dispersoids identified by SAED (inset in Fig. 10(a)) were observed in the BF image of the T6-treated 7055 plate. Highly dense η′ precipitates and Al_3(Sc,Zr) particles were also observed in the T6-treated 7055–*x*Zr–*y*Sc plates, in which some of the Al_3(Sc,Zr) particles were present in the GBs and dislocations (Figs. 10(b) and 10(c)). The size and density of the Al_3(Sc,Zr) particles in the 7055–*x*Zr–*y*Sc plates after the T6 treatment

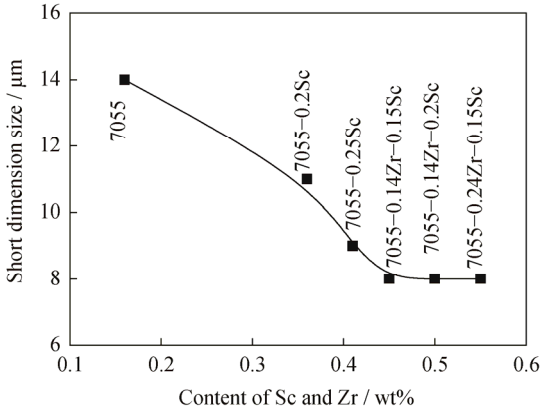

Fig. 9. Effect of Sc and Zr content on the short dimension size of samples after rolling and T6 treatment.

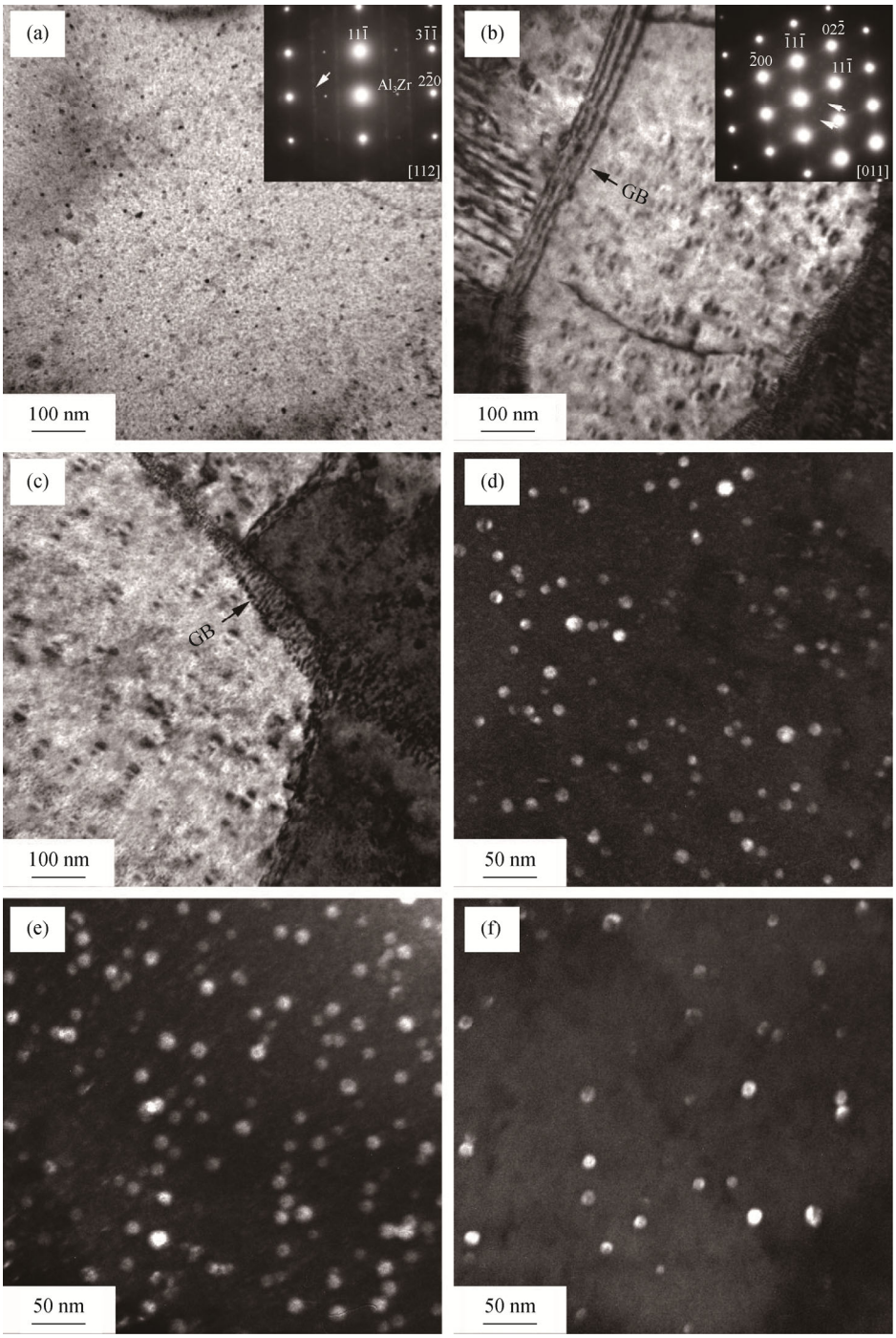

Fig. 10. TEM BF images of rolled plates: (a) 7055; (b) 7055–0.25Sc; (c) 7055–0.24Zr–0.15Sc, and DF images of alloys after rolling and T6 treatment: (d) 7055–0.25Sc; (e) 7055–0.14Zr–0.15Sc; (f) 7055–0.24Zr–0.15Sc. The arrows in the inserts of (a) and (b) denote the diffraction spot of the η′ phase.

were evaluated by TEM dark-field (DF) imaging. The reflection of the $Al_3(Sc,Zr)$ phase was used during imaging. Highly dense spherical $Al_3(Sc,Zr)$ particles with sizes of 6–18 nm were observed in all of the T6-treated 7055–*x*Zr–*y*Sc plates (Figs. 10(d)–10(f)).

Fig. 11 shows the size distributions of the $Al_3(Sc,Zr)$ phase in the T6-treated 7055–*x*Zr–*y*Sc rolled plates. The particle size distribution of 11–13 nm were dominant in the three samples, and the amount of $Al_3(Sc,Zr)$ particles with size larger than 13 nm increased with increasing total mass fraction of Sc and Zr in the 7055–*x*Zr–*y*Sc plates.

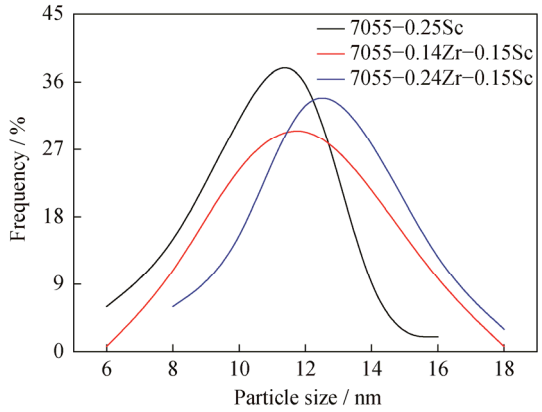

Fig. 11. Size distributions of the $Al_3(Sc,Zr)$ phase in 7055–*x*Zr–*y*Sc alloys after rolling and T6 treatment.

Fig. 12 shows the STEM high-angle annular dark-field (HAADF) images and the corresponding EDS maps of the T6-treated 7055 and 7055–0.25Sc rolled plates. The T6-treated 7055 plate contained θ-phase (Fig. 12(a)), and the EDS results showed that the large particles in the STEM-HAADF image of the T6-treated 7055–0.25Sc plates were in the θ- and W-phases (Fig. 12(b)).

Fig. 13 shows SEM images of the 7055–0.24Zr–0.15Sc rolled plates with different region after the T6 treatment. Micron-sized second phases were observed in this sample. The EDS results revealed that the A particles in region 1 (Fig. 13(a)) contained 64at% Al, 32at% Cu, and 4at% Sc, which corresponds to the W-phase. The B particles in region 2 (Fig. 13(b)) contained 75at% Al, 21at% Zr, and 4at% Sc. This composition and particle size correspond to the primary $Al_3(Sc,Zr)$ phase.

The recrystallization of 7055 rolled plates during the T6 treatment was substantially influenced by the Sc and Zr addition. The $Al_3(Sc,Zr)$ particles located at the GBs strongly pinned the GBs of the 7055–*x*Zr–*y*Sc plates during solution treatment, thereby inhibiting recrystallization and extensive grain growth (Figs. 10(b) and 10(c)).

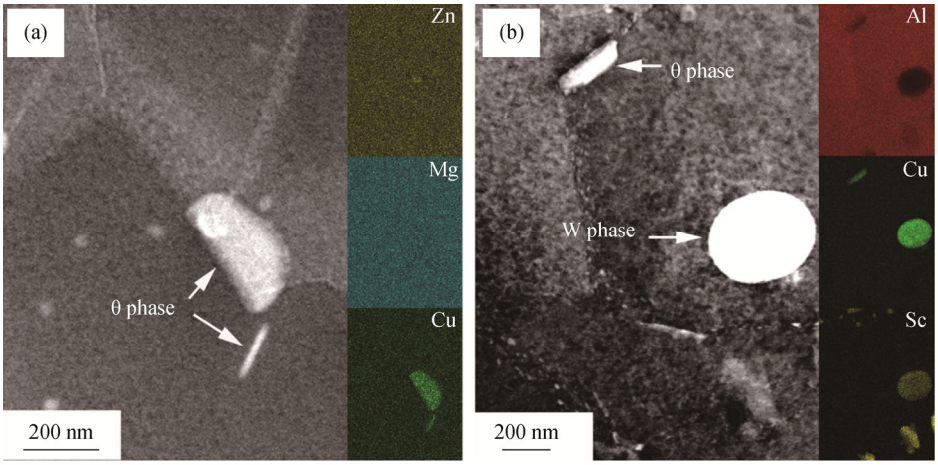

Fig. 12. STEM-HAADF images and corresponding EDS maps of (a) 7055 and (b) 7055–0.25Sc alloys after rolling and T6 treatment.

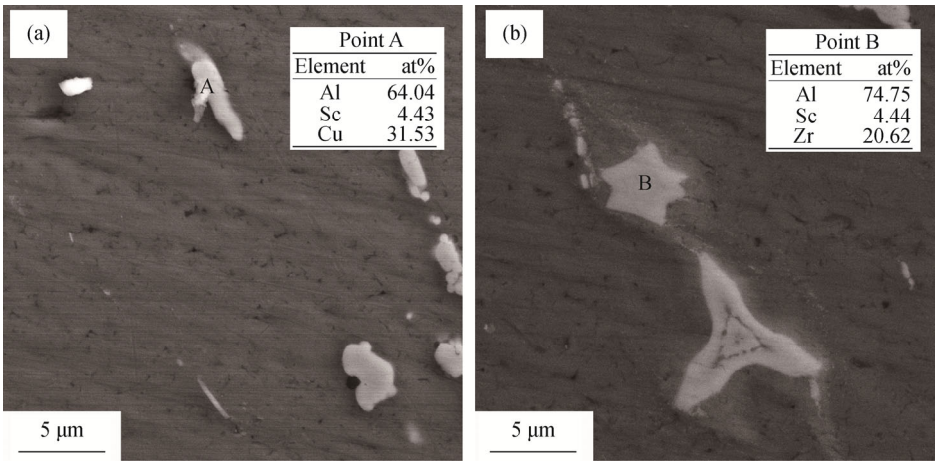

Fig. 13. SEM images of the 7055–0.24Zr–0.15Sc alloy after rolling and T6 treatment: (a) region 1; (b) region 2.

The high total mass fraction of Sc and Zr coarsened the precipitated $Al_3(Sc,Zr)$ phase (Fig. 11), and the W-phase (Fig. 12(b)) and primary $Al_3(Sc,Zr)$ phase (Fig. 13) consumed a substantial amount of Sc and Zr atoms and thereby inhibited the increase in the density of the precipitated $Al_3(Sc,Zr)$ phase. Thus, the excessive addition of Sc and Zr (total mass fraction of them larger than 0.45wt%) did not result in further grain refinement in the T6-treated 7055–*x*Zr–*y*Sc plates; the smallest average grain size in the 7055–*x*Zr–*y*Sc plates was approximately 8 μm when the total mass fraction of Sc and Zr was 0.45wt% (Fig. 9).

Table 3 shows the tensile properties of the T6-treated 7055 and 7055–*x*Zr–*y*Sc rolled plates. The addition of Sc improved the strength and ductility of the 7055 plate. The 7055–0.25Sc plate exhibited a higher ultimate tensile strength (UTS) and a greater elongation (EL) than the 7055–0.2Sc plate. The yield strength (YS) of the 7055 rolled plate was enhanced after the addition of Sc and Zr. However, only the 7055–0.14Zr–0.15Sc rolled plate exhibited superior mechanical properties than those of the 7055 rolled plate. Its YS, UTS, and EL reached 602 MPa, 657 MPa, and 13.8%, respectively. The addition of a large amount of Sc and Zr to the 7055 alloy deteriorated its UTS and EL.

Table 3. Tensile properties of 7055–*x*Zr–*y*Sc alloys after rolling and T6 treatment

7055–*x*Zr–*y*Sc	Total mass fraction of Sc and Zr / wt%	YS / MPa	UTS / MPa	EL / %
7055	0.16	577 ± 2	654 ± 2	12.8 ± 0.4
7055–0.2Sc	0.36	609 ± 2	649 ± 3	13 ± 0.5
7055–0.25Sc	0.41	600 ± 2	679 ± 2	14.3 ± 0.5
7055–0.14Zr–0.15Sc	0.45	602 ± 3	657 ± 4	13.7 ± 0.8
7055–0.14Zr–0.2Sc	0.5	593 ± 3	635 ± 5	10.3 ± 0.6
7055–0.24Zr–0.15Sc	0.55	580 ± 2	616 ± 3	7.3 ± 0.3

Fig. 14 shows the effect of the total mass fraction of Sc and Zr on the strength and ductility of the 7055–*x*Zr–*y*Sc rolled plates in the T6 state. The YS, UTS, and EL of the 7055–*x*Zr–*y*Sc plates increased initially with increasing total mass fraction of Sc and Zr, and then decreased. The samples with 0.41wt% (7055–0.25Sc plate) and 0.45wt% total mass fraction of Sc and Zr (7055–0.14Zr–0.15Sc plate) exhibited better mechanical properties than the 7055 plate.

The metastable η′ phase was the main strengthening phase in the T6-treated 7055 and 7055–*x*Zr–*y*Sc plates. All of the T6-treated 7055–*x*Zr–*y*Sc rolled plates exhibited a higher YS than the T6-treated 7055 rolled plate, primarily because the enhanced GBs and precipitation strengthening resulted from the fine grains (Figs. 8 and 9) and the increased density of the $Al_3(Sc,Zr)$ particles (Fig. 10).

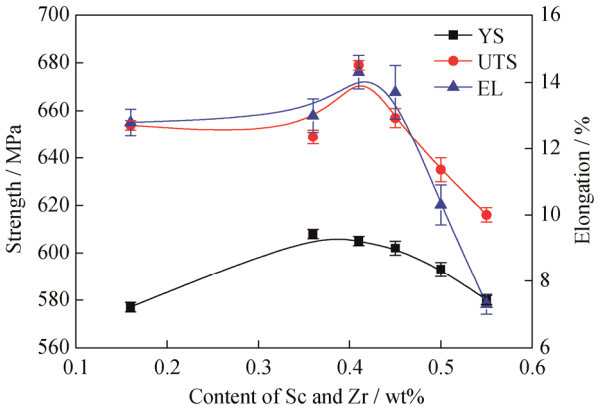

Fig. 14. Effect of Sc and Zr content on the tensile properties of 7055–*x*Zr–*y*Sc alloys after rolling and T6 treatment.

The strengthening effect of the precipitated $Al_3(Sc,Zr)$ phase on the 7055–*x*Zr–-*y*Sc plates decreased because of coarsening (Fig. 11) with increasing total mass fraction of Sc and Zr. When the total mass fraction of Sc and Zr exceeded 0.45wt%, the grain size maintained a constant value (Fig. 9), and the GBs strengthening effect stopped increasing with increasing total mass fraction of Sc and Zr. Thus, the net effect of high GBs and precipitation strengthening due to the $Al_3(Sc,Zr)$ precipitated phases considerably increased the strength of the 7055–0.25Sc plate.

Notably, the strength of the 7055–0.25Sc plate was only slightly higher than that of the 7055 plate because of the following factors: first, the precipitated $Al_3(Sc,Zr)$ particles were not the main strengthening phase in the 7xxx Al alloys, and the enhancement of precipitation strengthening was limited by the added Sc and Zr. Second, the GBs strengthening effect was not obvious in the Al alloys because of their low Hall-Petch parameters. Third, the W-phase deteriorated the mechanical properties of the high Cu content Al alloys.

After the T6 treatment, the grain sizes of the 7055–*x*Zr–*y*Sc rolled plates were much smaller than those of the 7055 rolled plate (Figs. 8 and 9), and the fine grains in the structure redistributed the stress, thereby preventing strain localization during tension and promoting high elongation before failure. Thus, minor Sc and Zr addition improved the ductility of the 7055 plate (Fig. 14).

The ductility of the 7055–*x*Zr–*y*Sc plates deteriorated when the total mass fraction of Sc and Zr was greater than 0.45wt%. The amount of the micron-sized primary coarse

Al_3(Sc,Zr) phase was extremely small in the T6-treated 7055–*x*Zr–*y*Sc plates (Fig. 13(b)) because of the low solubility of Zr and Sc in the Al matrix. Thus, the primary coarse Al_3(Sc,Zr) phase led to plastic instability and decreased ductility of the 7055–*x*Zr–*y*Sc plates. In the 7055–*x*Zr–*y*Sc plates with high total mass fraction of Sc and Zr, the dislocation–pinning effect of the precipitated Al_3(Sc,Zr) particles (Fig. 10) weakened because of their large sizes. Thus, the dislocation–accumulation capacities and work-hardening rates of Al alloys during tension decreased [33]. Consequently, the EL of the 7055–*x*Zr–*y*Sc plates decreased as well (Fig. 14).

4. Conclusions

The effect of Sc and Zr microalloying on the microstructure and mechanical properties of a 7xxx Al alloy with a high Cu content was investigated. The following conclusions were obtained:

(1) The addition of Sc and Zr to the 7055 alloy led to the formation of refined and equiaxed grains in the cast ingots. In the homogenized and T6-treated samples, Sc and Zr addition resulted in considerable grain refinement because of the effect of GBs pinning by the precipitated Al_3(Sc,Zr) phase. The Sc atoms diffused into the θ-phase and promoted the formation of the W-phase in the 7xxx Al alloy with a high Cu content.

(2) The peak aging time of the 7055 and 7055–*x*Zr–*y*Sc rolled plates ranged from 24 h to 26 h at 120°C, and the hardness of the 7055–*x*Zr–*y*Sc alloys was greater than that of the 7055 alloy.

(3) Minor additions of Sc and Zr improved the mechanical properties of the T6-treated 7055 plate because of the refined grains and increased density of the fine Al_3(Sc,Zr) phase. However, the W-phase and primary Al_3(Sc,Zr) phase, as well as the insufficient amount of refined grains, deteriorated the mechanical properties of the T6-treated 7055–*x*Zr–*y*Sc rolled plates when the total mass fraction of Sc and Zr exceeded 0.45wt%. The 7055–0.25Sc rolled plate exhibited the best mechanical properties among the prepared alloys.

Acknowledgements

This work was financially supported funded by the National Natural Science Foundation of China (No. 51601045), the Guangxi Natural Science Foundation (No. 2016GXNSFDA380028), and the Guangxi Science and Technology Major Project (No. GKAA17202007).

References

[1] Y. Buranova, V. Kulitskiy, M. Peterlechner, A. Mogucheva, R. Kaibyshev, S.V. Divinski, and G. Wilde, Al_3(Sc,Zr)-based precipitates in Al–Mg alloy: Effect of severe deformation, *Acta Mater.*, 124(2017), p. 210.

[2] T. Liu, C.N. He, G. Li, X. Meng, C.S. Shi, and N.Q. Zhao, Microstructural evolution in Al–Zn–Mg–Cu–Sc–Zr alloys during short-time homogenization, *Int. J. Miner. Metall. Mater.*, 22(2015), No. 5, p. 516.

[3] J.H. Li, M. Wiessner, M. Albu, S.Wurster, B. Sartory, F. Hofer, and P. Schumacher, Correlative characterization of primary Al_3(Sc,Zr) phase in an Al–Zn–Mg based alloy, *Mater. Charact.*, 102(2015), p. 62.

[4] M. Zhang, T. Liu, C.N. He, J. Ding, E.Z. Liu, C.S. Shi, J.J. Li, and N.Q. Zhao, Evolution of microstructure and properties of Al–Zn–Mg–Cu–Sc–Zr alloy during aging treatment, *J. Alloys Compd.*, 658(2016), p. 946.

[5] Y.L. Duan, G.F. Xu, L. Tang, Y. Liu, J.W. Xu, Y. Deng, and Z.M. Yin, Excellent high strain rate super plasticity of Al–Mg–Sc–Zr alloy sheet produced by an improved asymmetrical rolling process, *J. Alloys Compd.*, 715(2017), p. 311.

[6] B. Li, Q.L. Pan, X. Huang, and Z.M. Yin, Microstructures and properties of Al–Zn–Mg–Mn alloy with trace amounts of Sc and Zr, *Mater. Sci. Eng. A*, 616(2014), p. 219.

[7] X. Huang, Q.L. Pan, B. Li, Z.M. Liu, Z.Q. Huang, and Z.M. Yin, Microstructure, mechanical properties and stress corrosion cracking of Al–Zn–Mg–Zr alloy sheet with trace amount of Sc, *J. Alloys Compd.*, 650(2015), p. 805.

[8] G. Li, N.Q. Zhao, T. Liu, J.J. Li, C.N. He, C.S. Shi, E.Z. Liu, and J.W. Sha, Effect of Sc/Zr ratio on the microstructure and mechanical properties of new type of Al–Zn–Mg–Sc–Zr alloys, *Mater. Sci. Eng. A*, 617(2014), p. 219.

[9] Y. Deng, B. Peng, G.F. Xu, Q.L. Pan, Z.M. Yin, R. Ye, Y.J. Wang, and L.Y. Lu, Effects of Sc and Zr on mechanical property and microstructure of tungsten inert gas and friction stir welded aerospace high strength Al–Zn–Mg alloys, *Mater. Sci. Eng. A*, 639(2015), p. 500.

[10] C.Y. Liu, B. Zhang, Z.Y. Ma, G.B. Teng, L.L. Wei, W.B. Zhou, and X.Y. Zhang, Effects of pre-aging and minor Sc addition on the microstructure and mechanical properties of friction stir processed 7055 Al alloy, *Vacuum*, 149(2018), p. 106.

[11] Y. Chen, C.Y. Liu, B. Zhang, Z.Y. Ma, W.B. Zhou, H.J. Jiang, H.F. Huang, and L.L. Wei, Effects of friction stir processing and minor Sc addition on the microstructure, mechanical properties, and damping capacity of 7055 Al alloy, *Mater. Charact.*, 135(2018), p. 25.

[12] G.B. Teng, C.Y. Liu, Z.Y. Ma, W.B. Zhou, L.L. Wei, Y. Chen, J. Li, and Y.F. Mo, Effects of minor Sc addition on the microstructure and mechanical properties of 7055 Al alloy during aging, *Mater. Sci. Eng. A*, 713(2018), p. 61.

[13] C.Y. Liu, B. Zhang, Z.Y. Ma, H.J. Jiang, and W.B. Zhou, Effect of Sc addition, friction stir processing, and T6 treatment on the damping and mechanical properties of 7055 Al

alloy, *J. Alloys Compd.* 772(2019), p. 775.

[14] Z.H. Zhang, J. Xue, Y.B. Jiang, and F. Jin, Effect of pre-annealing treatment on the microstructure and mechanical properties of extruded Al–Zn–Mg–Cu alloy bars, *Int. J. Miner. Metall. Mater.*, 24(2017), No. 11, p. 1284.

[15] C.B. Cai, X.J. Xu, J.D. Huang, S.H. Ju, Q. Ding, and C.S. Wang, Effect of pre-recovery on microstructure and properties of rolled Al–12.18Zn–3.31Mg–1.43Cu–0.20Zr–0.04Sr aluminum alloy, *Int. J. Miner. Metall. Mater.*, 26(2019), No. 2, p. 241.

[16] C.B. Zheng, B.H. Yan, K. Zhang, and G. Yi, Electrochemical investigation on the hydrogen permeation behavior of 7075–T6 Al alloy and its influence on stress corrosion cracking, *Int. J. Miner. Metall. Mater.*, 22(2015), No. 7, p. 729.

[17] D. Wang, Z.Y. Ma, and Z.M. Gao, Effects of severe cold rolling on tensile properties and stress corrosion cracking of 7050 aluminum alloy, *Mater. Chem. Phys.*, 117(2009), No. 1, p. 228.

[18] J.F. Xie, Y.L. Zhu, F.L. Bian, and C. Liu, Dynamic recovery and recrystallization mechanisms during ultrasonic spot welding of Al–Cu–Mg alloy, *Mater. Charact.*, 132(2017), p. 145.

[19] S.K. Moghanaki, M. Kazeminezhad, and R. Logé, Effect of concurrent precipitation on the texture evolution during continuous heating of multi directionally forged solution treated Al–Cu–Mg alloy, *Mater. Charact.*, 131(2017), p. 399.

[20] I. Zuiko and R. Kaibyshev, Deformation structures and strengthening mechanisms in an Al–Cu alloy subjected to extensive cold rolling, *Mater. Sci. Eng. A*, 702(2017), p. 53.

[21] K. Yu, W.X. Li, S.R. Li, and J. Zhao, Mechanical properties and microstructure of aluminum alloy 2618 with $Al_3(Sc,Zr)$ phases, *Mater. Sci. Eng. A*, 368(2004), No. 1-2, p. 88.

[22] A.M. Samuel, S.A. Alkahtani, H.W. Doty, and F.H. Samuel, Role of Zr and Sc addition in controlling the microstructure and tensile properties of aluminum–copper based alloys, *Mater. Des.*, 88(2015), p. 1134.

[23] N.A. Belov, A.N. Alabin, and I.A. Matveeva, Optimization of phase composition of Al–Cu–Mn–Zr–Sc alloys for rolled products without requirement for solution treatment and quenching, *J. Alloys Compd.*, 583(2014), p. 206.

[24] M. Jia, Z.Q. Zheng, and Z. Gong, Microstructure evolution of the 1469 Al–Cu–Li–Sc alloy during, *J. Alloys Compd.*, 614(2014), p. 131.

[25] M. Gazizov, V. Teleshov, V. Zakharov, and R. Kaibyshev, Solidification behaviour and the effects of homogenisation on the structure of an Al–Cu–Mg–Ag–Sc alloy, *J. Alloys Compd.*, 509(2011), No. 39, p. 9497.

[26] Y.T. Li, Z.Y. Liu, Q.K. Xia, and Y.B. Liu, Grain refinement of the Al–Cu–Mg–Ag alloy with Er and Sc additions, *Metall. Mater. Trans. A*, 38(2007), No. 11, p. 2853.

[27] B.A. Chen, L. Pan, R.H. Wang, G. Liu, P.M. Cheng, L. Xiao, and J. Sun, Effect of solution treatment on precipitation behaviors and age hardening response of Al–Cu alloys with Sc addition, *Mater. Sci. Eng. A*, 530(2011), p. 607.

[28] L. Jiang, J.K. Li, G. Liu, R.H. Wang, B.A. Chen, J.Y. Zhang, J. Sun, M.X. Yang, G. Yang, J. Yang, and X.Z. Cao, Length-scale dependent microalloying effects on precipitation behaviors and mechanical properties of Al–Cu alloys with minor Sc addition, *Mater. Sci. Eng. A*, 637(2015), p. 139.

[29] S.D. Liu, X.M. Zhang, M.A. Chen, and J.H. You, Influence of aging on quench sensitivity effect of 7055 aluminum alloy, *Mater. Charact.*, 59(2008), No. 1, p. 53.

[30] J.R. Zuo, L.G. Hou, J.T. Shi, H. Cui, L.Z. Zhuang, and J.S. Zhang, The mechanism of grain refinement and plasticity enhancement by an improved thermomechanical treatment of 7055 Al alloy, *Mater. Sci. Eng. A*, 702(2017), p. 42.

[31] Y.X. Chen, Y.Q. Yang, Z.Q. Feng, B. Huang, and X. Luo, Surface gradient nanostructures in high speed machined 7055 aluminum alloy, *J. Alloys Compd.*, 726(2017), p. 367.

[32] H. She, D. Shu, J. Wang, and B.D. Sun, Influence of multi-microstructural alterations on tensile property inhomogeneity of 7055 aluminum alloy medium thick plate, *Mater. Charact.*, 113(2016), p. 189.

[33] Y.H. Zhao, X.Z. Liao, S. Cheng, E. Ma, and Y.T. Zhu, Simultaneously increasing the ductility and strength of nanostructured alloys, *Adv. Mater.*, 18(2006), p. 2280.